

Simulation Method and Code Development for Non-Axisymmetric Eddy Currents on Vacuum Vessels

Yushiro YAMASHITA, Yuji NAKAMURA, Akihiro ISHIZAWA and Kiyomasa WATANABE¹⁾

Graduate School of Energy Science, Kyoto University, Kyoto 611-0011, Japan

¹⁾*National Institute for Fusion Science, Toki, Gifu 509-5292, Japan*

(Received 26 July 2022 / Accepted 22 September 2022)

An electric current is induced on the vacuum vessel when the toroidal current of a tokamak plasma varies in time, and it is called the eddy current. During disruption, the eddy current becomes large and influences the process of disruption by interacting with the confined plasma. We have developed a new non-axisymmetric eddy current simulation code, the Keddy3D that solves the eddy current equation based on the thin-wall approximation. The Keddy3D is suitable for simulating long-term non-axisymmetric disruption processes with low computational costs.

© 2022 The Japan Society of Plasma Science and Nuclear Fusion Research

Keywords: tokamak, eddy current, numerical simulation, disruption

DOI: 10.1585/pfr.17.1403104

1. Introduction

Disruption is a sudden loss of plasma current in tokamaks and is one of the most critical issues for the practical use of the tokamak fusion reactor. In principle, a tokamak requires a plasma current, and the time variation of the current generates an inductive electric current in the surrounding conductors such as the vacuum vessel. The induced current on the vessel is called the eddy current and generates a magnetic field to interact with the plasma. During the disruption, the rapid loss of plasma current generates large eddy currents that are thought to affect the disruption process. Although experimental observations have shown that the disruption exhibits non-axisymmetry [1], the mechanism of non-axisymmetric disruption has not yet been fully understood. One of the reasons for this is a lack of understanding of non-axisymmetric eddy currents excited on the vacuum vessel.

Eddy currents are not unique to the nuclear fusion field but are a ubiquitous phenomenon of electromagnetism, and various analysis methods are developed. On the other hand, the vacuum vessel of a tokamak device has a specific geometry with periodicity in both poloidal and toroidal directions, which requires ingenuity in the eddy current analysis. In the eddy current calculations of axisymmetric disruption simulation codes such as DINA code [2], the vacuum vessel is modeled as a collection of axisymmetric multi-filaments, but this modeling is not applicable for the analysis of non-axisymmetric cases, and a different method must be employed.

In the study of non-axisymmetric disruption, the thin-wall approximation is usually employed by assuming that the thickness of the peripheral conductors is sufficiently

thin relative to the overall device scale. An example of an existing simulation code using this approximation for non-axisymmetric calculations of eddy currents is the EDDYCAL code [3, 4]. The EDDYCAL constructs equations based on the energy principle for a conductor system mesh divided by the finite element method and performs eigenvalue decomposition to obtain eddy currents expanded to a finite number of eigenmodes. While the finite element method can describe spatial structures with greater flexibility, its calculation process is more complicated than a simple finite difference method, and the calculation load tends to be heavy. EDDYCAL employs eigenmode expansion to enable time-evolving computations with low computational cost, but there is a tradeoff: a small number of modes restricts expressive ability, while a large number of modes demands a large amount of computation. In disruption analysis, it is necessary to perform a long-time analysis on the scale of transport phenomena while taking into account dynamically changing plasma currents. Thus an eddy current calculation code with reasonable expressive ability and light computational load is required. In addition, it is preferable to adopt a simple calculation method with high extensibility to deal with phenomena such as halo currents in the future. Based on this motivation, we have developed a simple eddy current calculation code based on the finite difference method.

In this study, we reformulate a computational theory of non-axisymmetric eddy currents based on the thin-wall approximation. Our computational theory is simpler, lighter-loaded, and suitable for disruption analysis compared to the EDDYCAL. A new simulation code, Keddy3D, was developed based on our computational theory and validated by numerical experiments. Our code is useful for the analysis of non-axisymmetric disruptions

author's e-mail: yamashita.yuushirou.33c@st.kyoto-u.ac.jp

and resistive wall modes (RWMs) [5].

This paper is composed of five sections. In Sec. 2, the computational theory of time evolution of non-axisymmetric eddy currents is described. In Sec. 3, the simulation code developed based on the theory is validated by numerical experiments. In Sec. 4, we discuss the limitation of our method on the application. Finally, in Sec. 5, we summarize the results.

2. Derivation of Eddy Current Equation and Numerical Method

In this section, we first develop the eddy current equation and then describe how its numerical solution works. The thin-wall approximation is described in Sec. 2.1, along with an overview of the coordinate system and eddy current representation form. To determine the temporal evolution of the non-axisymmetric eddy current distribution, the eddy current equation is derived in Sec. 2.2. The eddy current equation is discretized in Sec. 2.3 to solve them numerically. The discrete formulations for the spatial coordinates and the stream function are discussed in Secs. 2.3.1 and 2.3.2. Sections 2.3.3, 2.3.4, and 2.3.5 provide spatially discrete formulations for the terms of the magnetic field generated by eddy currents, magnetic field diffusion in the conductor, and magnetic field related to external sources, respectively. The temporal discretization and time evolution techniques are covered in Sec. 2.3.6. The boundary conditions that enable the system of equations to be solved are covered in Sec. 2.4, which also organizes the relation between the number of equations and the number of unknowns. We cover the computations for the unusual circumstances where the conductor is not periodic and the conductor shape is not smooth, respectively, in Secs. 2.5 and 2.6.

2.1 Thin-wall approximation

The vacuum vessel is considered as a surface without thickness in the thin-wall approximation, the current distribution in the radial direction is disregarded, and eddy currents are calculated as surface currents. This allows the vessel to be expanded into a two-dimensional grid with poloidal and toroidal coordinates, and the eddy currents to be represented by the gradient of a scalar potential, allowing for easier analysis. On the other hand, because it cannot manage the radial distribution, it may not be appropriate for analyses that reproduce the intricate dynamics around the divertor or for analyses where radial current diffusion is essential.

Consider a vacuum vessel in a curvilinear coordinate system (s, θ, ζ) . Let s be the minor radial coordinate with ∇s as the outward normal vector of the vessel, θ be the poloidal angle, and ζ be the toroidal angle. Assuming that a vacuum vessel of thickness d is approximated by a thin wall and that a surface current of surface current density \mathbf{J} is flowing on the thin wall, the current density \mathbf{j} is expressed as

pressed as

$$\mathbf{j} = \frac{\mathbf{J}}{d}. \quad (1)$$

According to the thin-wall approximation, the surface currents flow only in the θ and ζ directions. Therefore,

$$\mathbf{J} \cdot \nabla s = J^s = 0, \quad (2)$$

$$\mathbf{J} = J^\theta \mathbf{e}_\theta + J^\zeta \mathbf{e}_\zeta, \quad (3)$$

where \mathbf{e}_θ and \mathbf{e}_ζ are covariant basis vectors in the θ and ζ directions, and J^s, J^θ, J^ζ are the contravariant components in each directions. Any position \mathbf{r} in the Cartesian coordinate system (x, y, z) is

$$\mathbf{r} = x\hat{\mathbf{e}}_x + y\hat{\mathbf{e}}_y + z\hat{\mathbf{e}}_z, \quad (4)$$

where $\hat{\mathbf{e}}_x, \hat{\mathbf{e}}_y, \hat{\mathbf{e}}_z$ are the unit vectors in Cartesian coordinates. Then, \mathbf{e}_θ and \mathbf{e}_ζ can be expressed as follows,

$$\mathbf{e}_\theta = \frac{\partial \mathbf{r}}{\partial \theta} = \frac{\partial x}{\partial \theta} \hat{\mathbf{e}}_x + \frac{\partial y}{\partial \theta} \hat{\mathbf{e}}_y + \frac{\partial z}{\partial \theta} \hat{\mathbf{e}}_z, \quad (5)$$

$$\mathbf{e}_\zeta = \frac{\partial \mathbf{r}}{\partial \zeta} = \frac{\partial x}{\partial \zeta} \hat{\mathbf{e}}_x + \frac{\partial y}{\partial \zeta} \hat{\mathbf{e}}_y + \frac{\partial z}{\partial \zeta} \hat{\mathbf{e}}_z. \quad (6)$$

Defining contravariant basis vector ∇s with \mathbf{e}_θ and \mathbf{e}_ζ

$$\nabla s \equiv \frac{\mathbf{e}_\theta \times \mathbf{e}_\zeta}{|\mathbf{e}_\theta \times \mathbf{e}_\zeta|}, \quad (7)$$

the Jacobian determinant of the transformation \sqrt{g} can be defined as

$$\sqrt{g} = |\mathbf{e}_\theta \times \mathbf{e}_\zeta|. \quad (8)$$

Since eddy currents are induced currents,

$$\nabla \cdot \mathbf{J} = 0, \quad (9)$$

must always be satisfied. The partial derivatives with θ and ζ of the coordinate values at each position in equations such as (5) are provided exactly in our code since the form of the vacuum vessel is handled in the Fourier series expansion of cylindrical coordinates (R, ζ, Z) as

$$R(\theta, \zeta) = \sum_{k,l} R_{k,l}^c \cos(k\theta - l\zeta) + R_{k,l}^s \sin(k\theta - l\zeta), \quad (10)$$

$$Z(\theta, \zeta) = \sum_{k,l} Z_{k,l}^c \cos(k\theta - l\zeta) + Z_{k,l}^s \sin(k\theta - l\zeta), \quad (11)$$

where $x = R \cos \zeta, y = R \sin \zeta, z = Z$ in Cartesian coordinates.

As an expression that always satisfies Eq. (2), we consider the expression of the surface current density \mathbf{J} as the outer product of ∇s and a vector. Since the outer product

between gradient vectors has no divergence, by considering the expression (9) and introducing the stream function T , we obtain

$$\mathbf{J} = \nabla T \times \nabla s \quad (12)$$

$$= \frac{1}{\sqrt{g}} \frac{\partial T}{\partial \zeta} \mathbf{e}_\theta - \frac{1}{\sqrt{g}} \frac{\partial T}{\partial \theta} \mathbf{e}_\zeta. \quad (13)$$

Comparing this expression with (3), we obtain

$$J^\theta = \frac{1}{\sqrt{g}} \frac{\partial T}{\partial \zeta}, \quad (14)$$

$$J^\zeta = -\frac{1}{\sqrt{g}} \frac{\partial T}{\partial \theta}. \quad (15)$$

As a result, the time evolution of the stream function T should be determined to get the time evolution of eddy currents.

2.2 Eddy current equation

We begin the deriving process of the eddy current equation, which describes the time evolution of eddy currents with Faraday-Maxwell's equation

$$\frac{\partial \mathbf{B}}{\partial t} = -\nabla \times \mathbf{E}, \quad (16)$$

and Ohm's law

$$\mathbf{j} = \sigma \mathbf{E}, \quad (17)$$

as the starting equation, where σ is the conductivity of the vacuum vessel, \mathbf{B} is the magnetic field vector, and \mathbf{E} is the electric field vector. From Eqs. (16) and (17),

$$\frac{\partial \mathbf{B}}{\partial t} = -\nabla \times \left(\frac{\mathbf{J}}{\sigma d} \right), \quad (18)$$

is obtained, where the magnetic field is

$$\mathbf{B} = \mathbf{B}_{\text{eddy}} + \mathbf{B}_{\text{ex}}. \quad (19)$$

Here, \mathbf{B}_{eddy} is the magnetic field generated by the eddy currents and \mathbf{B}_{ex} by the external sources. If \mathbf{B}_{eddy} and \mathbf{B}_{ex} are separated as shown, (18) can be written as

$$\frac{\partial \mathbf{B}_{\text{eddy}}}{\partial t} = -\nabla \times \left(\frac{\mathbf{J}}{\sigma d} \right) - \frac{\partial \mathbf{B}_{\text{ex}}}{\partial t}. \quad (20)$$

This Eq. (20) is the basic form of the eddy current equation. Furthermore, \mathbf{B}_{eddy} can be written from Biot-Savart's law as

$$\begin{aligned} \mathbf{B}_{\text{eddy}} &= \frac{\mu_0}{4\pi} \iiint \frac{\mathbf{j} \times (\mathbf{r} - \mathbf{r}')}{|\mathbf{r} - \mathbf{r}'|^3} \sqrt{g} ds' d\theta' d\zeta' \\ &= \frac{\mu_0}{4\pi} \iiint \frac{\mathbf{J} \times (\mathbf{r} - \mathbf{r}')}{|\mathbf{r} - \mathbf{r}'|^3} \sqrt{g} d\theta' d\zeta', \end{aligned} \quad (21)$$

where \mathbf{r}' , ds' , $d\theta'$, $d\zeta'$ denote variables at the position of the current element. Substituting Eq. (21) into (20), we obtain the eddy current equation

$$\begin{aligned} \frac{\partial}{\partial t} \left[\frac{\mu_0}{4\pi} \iiint \frac{\mathbf{J} \times (\mathbf{r} - \mathbf{r}')}{|\mathbf{r} - \mathbf{r}'|^3} \sqrt{g} d\theta' d\zeta' \right] \\ = -\nabla \times \left(\frac{\mathbf{J}}{\sigma d} \right) - \frac{\partial \mathbf{B}_{\text{ex}}}{\partial t}. \end{aligned} \quad (22)$$

The rotation of any vector \mathbf{A} in curvilinear coordinates is expressed as

$$\nabla \times \mathbf{A} = \sum_i \left(\sum_{j,k} \frac{1}{\sqrt{g}} \varepsilon_{ijk} \frac{\partial A_k}{\partial u_j} \right) \mathbf{e}_i. \quad (23)$$

Therefore, the first term on the right-hand side of the Eq. (22) at the (s, θ, ζ) coordinates can be rewritten as

$$\nabla \times \mathbf{J} = \frac{1}{\sqrt{g}} \left[\left(\frac{\partial J_\zeta}{\partial \theta} - \frac{\partial J_\theta}{\partial \zeta} \right) \mathbf{e}_s \left(\mathbf{e}_\theta \frac{\partial}{\partial \zeta} - \mathbf{e}_\zeta \frac{\partial}{\partial \theta} \right) J_s \right], \quad (24)$$

where J_θ and J_ζ are the covariant components of \mathbf{J} in θ and ζ directions, and \mathbf{J} has no radial distribution. Only the components in the \mathbf{e}_s direction are connected to the surface currents J^θ and J^ζ , according to the Eq. (24). Therefore, we ignore the eddy current equation of \mathbf{e}_θ and \mathbf{e}_ζ direction. Taking the inner product of the entire Eq. (22) and ∇s , we obtain

$$\begin{aligned} \frac{\partial}{\partial t} \left[\frac{\mu_0}{4\pi} \iint \frac{\mathbf{J} \times (\mathbf{r} - \mathbf{r}') \cdot \nabla s}{|\mathbf{r} - \mathbf{r}'|^3} \sqrt{g} d\theta' d\zeta' \right] \\ = -\nabla \times \left(\frac{\mathbf{J}}{\sigma d} \right) \cdot \nabla s - \frac{\partial \mathbf{B}_{\text{ex}} \cdot \nabla s}{\partial t}, \end{aligned} \quad (25)$$

which we actually need to solve. This Eq. (25) represents the s -direction component of the eddy current equation. This equation will be referred to as the eddy current equation throughout this paper.

2.3 Discretization of eddy current equation

The eddy current Eq. (25) must be discretized and solved numerically because it cannot be solved analytically. The specifics of the numerical calculation are described in this section.

2.3.1 Spatial grid

The θ - ζ surface on which the vacuum vessel is placed is divided into a grid with fixed intervals of $\Delta\theta$ and $\Delta\zeta$ in each direction. Using the indices i and j , the position of a grid point is then determined as

$$\theta_i = \Delta\theta(i - 1), \quad (26)$$

$$\zeta_j = \Delta\zeta(j - 1). \quad (27)$$

When the number of grid points in the θ direction is m and in the ζ direction is n , $\Delta\theta = 2\pi/m$ and $\Delta\zeta = 2\pi/n$.

The left side of Eq. (22) diverges to infinity when the evaluation position of the magnetic field \mathbf{r} and the position of the current element \mathbf{r}' are identical. Therefore, a staggered mesh is employed so that the evaluation grid does not overlap with the current grid. As an example, a staggered mesh is shown in Fig. 1 when the number of grid points is $(m, n) = (3, 3)$. When the base position of each grid $(\theta, \zeta) = (\theta_i, \zeta_j)$, the evaluation points for the magnetic field and stream function are $(\theta, \zeta) = (\theta_i + \frac{\Delta\theta}{2}, \zeta_j + \frac{\Delta\zeta}{2})$, the evaluation point of poloidal current is $(\theta, \zeta) = (\theta_i + \frac{\Delta\theta}{2}, \zeta_j)$ and the evaluation point of toroidal current is $(\theta, \zeta) = (\theta_i, \zeta_j + \frac{\Delta\zeta}{2})$.

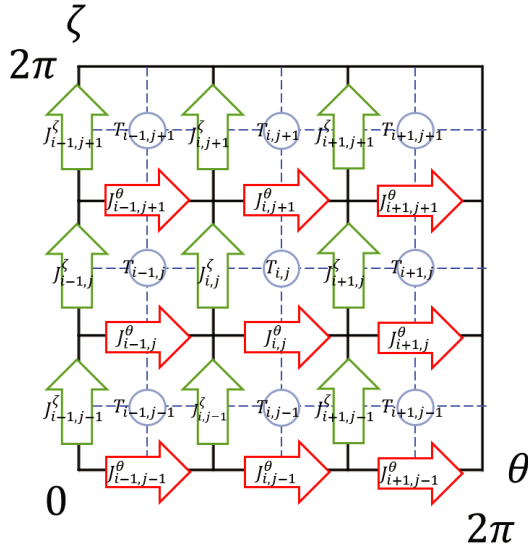


Fig. 1 Example of staggered mesh with the number of grid points $(m, n) = (3, 3)$.

2.3.2 Stream function

Considering the expressions (14) and (15) on the discrete grid, we obtain

$$J_{i,j}^{\theta} = \frac{1}{\sqrt{g_{i,j}}} \frac{T_{i,j} - T_{i,j-1}}{\Delta \zeta}, \quad (28)$$

$$J_{i,j}^{\zeta} = -\frac{1}{\sqrt{g_{i,j}}} \frac{T_{i,j} - T_{i-1,j}}{\Delta \theta}, \quad (29)$$

where the Jacobian \sqrt{g} is the value at each current position. \mathbf{J} and T are handled as one-dimensional arrays $[J^{\theta}]$, $[J^{\zeta}]$ and $[T]$ in programming. Then, the transformation of \mathbf{J} and T is implemented as:

$$[J^{\theta}] = [M_{J^{\theta}T}][T], \quad (30)$$

$$[J^{\zeta}] = [M_{J^{\zeta}T}][T], \quad (31)$$

where $[M_{J^{\theta}T}]$ and $[M_{J^{\zeta}T}]$ are the coefficient matrices.

Looking at Eqs. (28) and (29), we notice that it is necessary to refer to the value of the off-grid stream function whose index is 0 to determine the surface current at the minimum end of the grid ($j = 1$ in Eq. (28) and $i = 1$ in Eq. (29)). Due to the periodicity of the torus, the point with index 0 physically represents the same position as the point with the maximum index, hence, all physical quantities at θ_0 and θ_m , ζ_0 and ζ_n must have the same value. The stream function, unlike the Jacobian and surface currents, is not periodic since it is not a physical quantity. Thus, the value of the stream function at index 0 can differ from the value at the maximum index. On the other hand, if the value of the stream function at each one point with $i = 0$ and $j = 0$ is known, the surface currents at the maximum index can be used to obtain the stream function values at all remaining outer-grid points because the surface currents represent

the gradient of the stream function. Specifically, by substituting $i = 0$ into Eq. (28) and transforming it, we obtain

$$T_{0,j} = T_{0,j-1} + T_{m,j} - T_{m,j-1}. \quad (32)$$

For example, when the value of $T_{0,1}$ is known, we obtain the expression for $T_{0,j}$ as

$$T_{0,j} = T_{0,1} + T_{m,j} - T_{m,1}, \quad (33)$$

where the right-hand side is composed of the known values and the values in the grid. As similarly for $j = 0$, if $T_{1,0}$ is known

$$T_{i,0} = T_{1,0} + T_{i,n} - T_{1,n}, \quad (34)$$

can be said. Therefore, in order to represent J^{θ} and J^{ζ} for all grid points, the stream function array needs to include $T_{0,1}$ and $T_{1,0}$ in $[T]$.

Because the stream function is a potential, even if the gradient (surface current) is known, the value cannot be determined without a reference point. Any point can be taken as the reference, but we choose $T_{m,n} = 0$ in this case. In summary, the unknowns to be sought to represent the eddy currents are $[T_{1,1}, T_{2,1}, \dots, T_{m,1}, T_{1,2}, \dots, T_{m-1,n}, T_{0,1}, T_{1,0}]$, the number of which is $m \times n + 1$.

2.3.3 Eddy current field term

Consider the discrete form of the left-hand side of the eddy current Eq. (25), the term for the magnetic field generated by the eddy currents. Since the calculation of the outer product of vectors is simplified in Cartesian coordinates, we handle $\mathbf{J} \times (\mathbf{r} - \mathbf{r}') \cdot \nabla_s$ in Cartesian coordinates. From the expressions (3), (5) and (6), the eddy current vector \mathbf{J} can be written as

$$\begin{aligned} \mathbf{J} = & \left(J^{\theta} \frac{\partial x}{\partial \theta} + J^{\zeta} \frac{\partial x}{\partial \zeta} \right) \hat{\mathbf{e}}_x \\ & + \left(J^{\theta} \frac{\partial y}{\partial \theta} + J^{\zeta} \frac{\partial y}{\partial \zeta} \right) \hat{\mathbf{e}}_y \\ & + \left(J^{\theta} \frac{\partial z}{\partial \theta} + J^{\zeta} \frac{\partial z}{\partial \zeta} \right) \hat{\mathbf{e}}_z, \end{aligned} \quad (35)$$

$$J_x \equiv J^{\theta} \frac{\partial x}{\partial \theta} + J^{\zeta} \frac{\partial x}{\partial \zeta}, \quad (36)$$

$$J_y \equiv J^{\theta} \frac{\partial y}{\partial \theta} + J^{\zeta} \frac{\partial y}{\partial \zeta}, \quad (37)$$

$$J_z \equiv J^{\theta} \frac{\partial z}{\partial \theta} + J^{\zeta} \frac{\partial z}{\partial \zeta}. \quad (38)$$

Then the outer product of the current vector and relative position vector is

$$\mathbf{J} \times (\mathbf{r} - \mathbf{r}') = \rho_x \hat{\mathbf{e}}_x + \rho_y \hat{\mathbf{e}}_y + \rho_z \hat{\mathbf{e}}_z, \quad (39)$$

where

$$\rho_x \equiv J_y (z - z') - J_z (y - y'), \quad (40)$$

$$\rho_y \equiv J_z (x - x') - J_x (z - z'), \quad (41)$$

$$\rho_z \equiv J_x (y - y') - J_y (x - x'). \quad (42)$$

Now $\mathbf{J} \times (\mathbf{r} - \mathbf{r}')$ is expressed in Cartesian coordinates. The remaining ∇s can be obtained from the definition (7),

$$\begin{aligned} \nabla s &= \frac{1}{\sqrt{g}} \left(\frac{\partial y}{\partial \theta} \frac{\partial z}{\partial \zeta} - \frac{\partial z}{\partial \theta} \frac{\partial y}{\partial \zeta} \right) \hat{\mathbf{e}}_x \\ &+ \frac{1}{\sqrt{g}} \left(\frac{\partial z}{\partial \theta} \frac{\partial x}{\partial \zeta} - \frac{\partial x}{\partial \theta} \frac{\partial z}{\partial \zeta} \right) \hat{\mathbf{e}}_y \\ &+ \frac{1}{\sqrt{g}} \left(\frac{\partial x}{\partial \theta} \frac{\partial y}{\partial \zeta} - \frac{\partial y}{\partial \theta} \frac{\partial x}{\partial \zeta} \right) \hat{\mathbf{e}}_z \\ &\equiv (\nabla s)_x \hat{\mathbf{e}}_x + (\nabla s)_y \hat{\mathbf{e}}_y + (\nabla s)_z \hat{\mathbf{e}}_z. \end{aligned} \quad (43)$$

Thus, the numerator of the function under integration on the left-hand side of the Eq. (25) becomes

$$\mathbf{J} \times (\mathbf{r} - \mathbf{r}') \cdot \nabla s = \rho_x (\nabla s)_x + \rho_y (\nabla s)_y + \rho_z (\nabla s)_z. \quad (44)$$

If we again divide this into the coefficients over J^θ and J^ζ , we can express $\mathbf{J} \times (\mathbf{r} - \mathbf{r}')$ as the product of coefficient matrix and vector:

$$[L] = [M_{LJ^\theta}] [J^\theta] + [M_{LJ^\zeta}] [J^\zeta], \quad (45)$$

where $[L]$ is an array representing the left-hand side term of the eddy current equation, which will be time-partially differentiated.

2.3.4 Diffusion term

The first term on the right-hand side of the eddy current Eq. (25) represents the magnetic field diffusion in the conductor. We discretize this term as follows. From the Eq. (24), the magnetic field diffusion term can be transformed as

$$\nabla \times \left(\frac{\mathbf{J}}{\sigma d} \right) \cdot \nabla s = \frac{1}{\sqrt{g}} \left[\frac{\partial}{\partial \theta} \left(\frac{J_\zeta}{\sigma d} \right) - \frac{\partial}{\partial \zeta} \left(\frac{J_\theta}{\sigma d} \right) \right]. \quad (46)$$

Using the covariant measurement tensor g , covariant components are expressed with contravariant components:

$$J_\theta = g_{\theta\theta} J^\theta + g_{\theta\zeta} J^\zeta, \quad (47)$$

$$J_\zeta = g_{\zeta\theta} J^\theta + g_{\zeta\zeta} J^\zeta. \quad (48)$$

Therefore, we obtain

$$\begin{aligned} &-\nabla \times \left(\frac{\mathbf{J}}{\sigma d} \right) \cdot \nabla s \\ &= -\frac{1}{\sqrt{g}} \left[\frac{\partial}{\partial \theta} \left(\frac{g_{\zeta\theta}}{\sigma d} J^\theta - \frac{g_{\zeta\zeta}}{\sigma d} J^\zeta \right) - \frac{\partial}{\partial \zeta} \left(\frac{g_{\theta\theta}}{\sigma d} J^\theta - \frac{g_{\theta\zeta}}{\sigma d} J^\zeta \right) \right]. \end{aligned} \quad (49)$$

This term can also be organized by separating the coefficient on J^θ and the coefficient on J^ζ as

$$[R] = [M_{RJ^\theta}] [J^\theta] + [M_{RJ^\zeta}] [J^\zeta], \quad (50)$$

where $[R]$ is an array representing the first term on the right-hand side of the eddy current equation.

2.3.5 External term

The second term on the right-hand side of the eddy current Eq. (25) is the term of the magnetic field generated by external currents and so on. In this paper, the magnetic fields generated by the plasma current and the center solenoid coil current are assumed to be included in this term.

The magnetic field generated by plasma current can be calculated by Biot-Savart's law in the same way as the term of the magnetic field generated by eddy currents. Plasma currents, unlike eddy currents, have a three-dimensional distribution and must be three-dimensionally integrated to obtain the magnetic field. To lessen the computational load, we adopt the Virtual Casing method (VC method) [6] in our code, which reduces the integration dimension by considering a virtual conductor surface. Note that the accuracy of the VC method tends to deteriorate when the plasma and the vessel are very close. When the distance to the plasma is less than a certain threshold, the VC method is not applied, and a 3-dimensional integration is performed in our code.

By modeling the center solenoid as an axisymmetric conductor, the magnetic field generated by the center solenoid current \mathbf{B}_{CS} can be computed using general elliptic integration. We then take an inner product of \mathbf{B}_{CS} and ∇s in (43) because what we want to evaluate is B_{CS}^s . Since the eddy current equation requires the time derivative of B^s , the magnetic field generated by the center solenoid current I_{CS} is calculated by giving known $\frac{\partial I_{CS}}{\partial t}$. For the magnetic field generated by the plasma current, it is necessary to obtain $\frac{\partial B_{ex}^s}{\partial t}$ by subtracting the magnetic field from the previous time step's value.

2.3.6 Integration scheme for time evolution

To determine the time evolution of the eddy currents, we perform temporal integration of T . Expressing the Eq. (25) in the form of the arrays, we obtain

$$\frac{\partial}{\partial t} [L] = [R] - \left[\frac{\partial B_{ex}^s}{\partial t} \right]. \quad (51)$$

Furthermore, from the expressions (30), (31), (45), and (50), $[L]$ and $[R]$ can be expressed as the product of $[T]$ and coefficient matrices:

$$\begin{aligned} [L] &= \{ [M_{LJ^\theta}] [M_{J^\theta T}] + [M_{LJ^\zeta}] [M_{J^\zeta T}] \} [T] \\ &\equiv [X] [T], \end{aligned} \quad (52)$$

$$\begin{aligned} [R] &= \{ [M_{RJ^\theta}] [M_{J^\theta T}] + [M_{RJ^\zeta}] [M_{J^\zeta T}] \} [T] \\ &\equiv [Y] [T]. \end{aligned} \quad (53)$$

$[X]$ is time-invariant because the coefficients depend only on the vessel shape. Then, the Eq. (51) can be rewritten as the time evolution equation for $[T]$:

$$[X] \frac{\partial}{\partial t} [T] = [Y] [T] - \left[\frac{\partial B_{ex}^s}{\partial t} \right]. \quad (54)$$

This expression (54) is the discrete form of the eddy current Eq. (25) and what our code solves. To obtain $[T]$ at the next time step, we multiply the inverted matrix of $[X]$ from the left and replace the time derivation with the numerical differentiation. If we apply a simple explicit method (Euler method), the Eq. (54) is solved as follows:

$$[T]_{t+\Delta t} = [T]_t + \Delta t [X]^{-1} \left([Y][T]_t - \left[\frac{\partial B_{\text{ex}}^s}{\partial t} \right] \right), \quad (55)$$

where the lower subscript denotes the time, t is the current time, and Δt is the time step of discretization. Note that $[X]$ must be a regular matrix for the inverse matrix to exist. The regularity of the matrix is discussed in Sec. 2.4.

Since the Eq. (54) is a linear problem, we can easily apply the implicit method to the problem to improve the stability of the solution. When we apply the Crank-Nicolson method, the Eq. (54) is solved as follows:

$$\begin{aligned} [T]_{t+\Delta t} &= \left([X] \frac{1}{\Delta t} - \frac{1}{2} [Y] \right)^{-1} \left[\left([X] \frac{1}{\Delta t} + \frac{1}{2} [Y] \right) [T]_t - \left[\frac{\partial B_{\text{ex}}^s}{\partial t} \right] \right]. \end{aligned} \quad (56)$$

Our code adopts the Crank-Nicolson method for temporal integration. The disadvantage of the implicit method is that the time step Δt is included in the coefficient matrix for which the inverse matrix should be calculated, so if the time increment is changed in the middle of the simulation, the inverse matrix calculation must be performed each time. Since the most computation time-consuming part of our code is the inverse matrix calculation, it may be more efficient to use the Euler method or the Runge-Kutta method if the time step is frequently changed during the simulation. However, the inverse matrix calculation is particularly time-consuming when the number of grid points is large, in which case the explicit method requires an even finer time step due to the Courant condition.

From the Eq. (54), the eddy current distribution at a steady state can be obtained directly. Since the time-varying term on the left-hand side is zero in the steady-state, the eddy currents under the steady-state time variation of the external magnetic field $\left[\frac{\partial B_{\text{ex}}^s}{\partial t} \right]$ can be calculated as

$$[T]_{\text{steady}} = [Y]^{-1} \left[\frac{\partial B_{\text{ex}}^s}{\partial t} \right]. \quad (57)$$

2.4 Boundary conditions and solvability

As mentioned in Sec. 2.3.2, if the number of the grid points is (m, n) in (θ, ζ) direction, there are $m \times n + 1$ unknowns to be obtained. On the other hand, the number of the eddy current equations is only $m \times n$ at most because it is a physical equation and can be established at each grid point. Furthermore, because the total flux linkage on the closed surface is zero (Faraday's law), the number of independent equations is restricted to $m \times n - 1$, since the magnetic field at one point is determined from the

magnetic fields at all other points. Therefore, as boundary conditions, the equations for the circulating voltage in the poloidal and toroidal directions are introduced.

$$V_{\text{pol}}^{\text{loop}} = \oint_{C_\theta} \frac{\partial \mathbf{A}}{\partial t} \cdot d\mathbf{l}_\theta = - \oint_{C_\theta} \left(\frac{\mathbf{J}}{\sigma d} \right) \cdot d\mathbf{l}_\theta, \quad (58)$$

$$V_{\text{tor}}^{\text{loop}} = \oint_{C_\zeta} \frac{\partial \mathbf{A}}{\partial t} \cdot d\mathbf{l}_\zeta = - \oint_{C_\zeta} \left(\frac{\mathbf{J}}{\sigma d} \right) \cdot d\mathbf{l}_\zeta, \quad (59)$$

where $V_{\text{pol}}^{\text{loop}}$ and $V_{\text{tor}}^{\text{loop}}$ are the circulating voltages in the poloidal and toroidal directions respectively, \mathbf{A} is the vector potential, C_θ and C_ζ are the integral loop, and \mathbf{l} is the line element along the integral loop. Separating the vector potential in the left-hand side term to the components generated by eddy currents and by external sources like (19), we obtain

$$\begin{aligned} \oint_{C_\theta} \frac{\partial \mathbf{A}_{\text{eddy}}}{\partial t} \cdot d\mathbf{l}_\theta &= - \oint_{C_\theta} \left(\frac{\mathbf{J}}{\sigma d} \right) \cdot d\mathbf{l}_\theta - \oint_{C_\theta} \frac{\partial \mathbf{A}_{\text{ex}}}{\partial t} \cdot d\mathbf{l}_\theta, \end{aligned} \quad (60)$$

$$\begin{aligned} \oint_{C_\zeta} \frac{\partial \mathbf{A}_{\text{eddy}}}{\partial t} \cdot d\mathbf{l}_\zeta &= - \oint_{C_\zeta} \left(\frac{\mathbf{J}}{\sigma d} \right) \cdot d\mathbf{l}_\zeta - \oint_{C_\zeta} \frac{\partial \mathbf{A}_{\text{ex}}}{\partial t} \cdot d\mathbf{l}_\zeta. \end{aligned} \quad (61)$$

We can use any loop to evaluate the circulating voltage, but if the point of evaluation of the vector potential coincides exactly with the location of the current element, the vector potential will diverge. In our code, the vector potential is evaluated on the $(\theta, \zeta) = (\theta_i, \zeta_j)$ grid so that it does not overlap with the current point. Since the voltage drop is evaluated in integral value, the value evaluated on the $(\theta, \zeta) = (\theta_i, \zeta_j)$ grid should be identical with the value evaluated on the current grid $(\theta, \zeta) = (\theta_i + \frac{\Delta\theta}{2}, \zeta_j)$ for poloidal direction and $(\theta, \zeta) = (\theta_i, \zeta_j + \frac{\Delta\zeta}{2})$ for toroidal direction. The Biot-Savart law for vector potential is

$$\mathbf{A}(\mathbf{r}) = \frac{\mu_0}{4\pi} \iint \frac{\mathbf{J}(\mathbf{r}')}{|\mathbf{r} - \mathbf{r}'|} \sqrt{g} d\theta' d\zeta', \quad (62)$$

and can be expressed in the same way as the magnetic field, by multiplying the stream function by the coefficient matrix.

To incorporate the Eqs. (60) and (61) into the eddy current Eq. (54), the term on the left-hand side and the second term on the right-hand side of the eddy current equation are extended to include the rows of coefficients for the vector potential generated by the eddy currents and external source respectively. To the first term on the right-hand side of the Eq. (54), we add the rows of coefficients representing the voltage drop due to electrical resistance and eddy currents as the corresponding quantities to the circular voltage. This results in a total of $m \times n + 1$ equations, which equals the number of unknowns, indicating that the system of equations is now solvable. All of these $m \times n + 1$ equations are independent, ensuring the regularities of the

matrices and the existence of the inverse matrices required by Eqs. (55) and (56).

Consider the physical meaning and computational role of the circulating voltage equation used for the boundary conditions. Physically, the integral of the eddy currents around the vessel is given by the circulating voltage equation, and the difference between eddy currents is given by the eddy current equation. They determine the current values at all points by working together. Computationally, the circulating voltage equation determines the difference of T from the value after one round of the vessel, so that T outside the grid can be fully represented by T inside the grid, and the eddy current equation becomes solvable. Figure 2 shows a schematic diagram that summarizes the theory up to this point. The number of unknowns is $m \times n - 1$ in the grid and 2 outside the grid, and the number of equations is $m \times n - 1$ in the eddy current equations and 2 in the circulating voltage equations, which constitute together a set of linear equations (matrix equations) of $m \times n + 1$ order.

2.5 Non-periodic spatial structure case

The calculation theory described up to Sec. 2.4 assumes a torus vessel with periodicity in the poloidal and toroidal directions, and it must be modified if the object to be calculated is a spatially non-periodic conductor, such as stabilizing plate [7]. In obtaining the eddy currents at the edge of the grid, the Eqs. (33) and (34) can be used when

there is periodicity. In the case of no periodicity at all, all the values of the off-grid stream function are identical, because no eddy currents (corresponding to the gradient of the stream function) flow outside the grid. Therefore, there is only one value of T outside the grid that should be considered as an unknown, and the number of unknowns is decreased to $m \times n$. Next, we consider the number of equations. Different from Sec. 2.4, the linear dependency of the eddy current equations which is due to the total flux linkage is eliminated because the conductor is not a closed surface. Thus, $m \times n$ eddy current equations are available. At this point, the number of equations coincides with the number of unknowns, indicating that the boundary conditions are no longer necessary.

Similarly, we evaluate the number of unknowns and equations for the case of periodicity in only one direction. For example, if the periodicity is in the θ direction, each one off-grid stream function value on the maximum side and the minimum side of ζ grid should be treated as unknown. When the periodicity is in the ζ direction, the result is the same. The total number of unknowns is thus $m \times n + 1$, which is the same as in the torus case and $m \times n$ eddy current equations are available as in the non-periodic case. Therefore, just one boundary condition, namely the circulating voltage equation, is needed.

2.6 Spatially non-differentiable structure case

The calculation theory described in Sec. 2.1 to Sec. 2.4 assumes that the conductor has a spatially smooth (differentiable) structure. In this section, we will look at how to calculate eddy currents in conductors with non-smooth spatial patterns.

Because the stream function and eddy current are mapped by spatial differentiation as (14) and (15), the representation by the stream function is not possible at points where the spatial derivative cannot be defined. Although the stream function representation guarantees to satisfy the continuity equation of surface current at each grid point, the continuity equation must be considered by other means if the stream function is not used. Consider the use of Kirchhoff's first law in a circuit network that imitates the grid on the conductor. If the net current at each grid intersection is zero, there is no divergence of current. A schematic diagram of the current inflow and outflow at an intersection is shown in Fig. 3.

To avoid confusion with the previous sections, we define α and β as arbitrary coordinate axes along the vessel surface in this section. Also, J^α and J^β are not the contravariant components of the surface currents, but the components of the physical surface currents in each direction. Because the surface current values after discretization are representative values around the grid point, the current flowing into the intersection can be obtained by taking the products of surface currents J^α, J^β and the grid widths

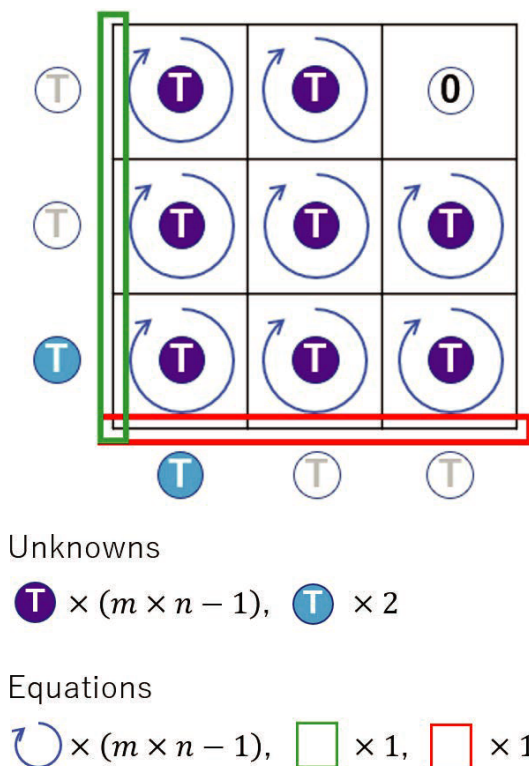


Fig. 2 Schematic diagram of the numbers of unknowns and independent equations on the eddy current calculation.

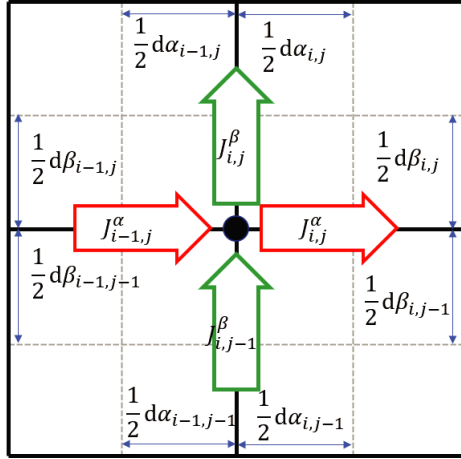


Fig. 3 Schematic diagram of the current inflow and outflow at an intersection on the circuit network.

$d\alpha$, $d\beta$. Thus, Kirchhoff's first law at the grid intersection (i, j) can be expressed as

$$\begin{aligned} J_{i-1,j}^\alpha (d\beta_{i-1,j-1} + d\beta_{i-1,j}) + J_{i,j-1}^\beta (d\alpha_{i-1,j-1} + d\alpha_{i,j-1}) \\ - J_{i,j}^\alpha (d\beta_{i,j-1} + d\beta_{i,j}) - J_{i,j}^\beta (d\alpha_{i-1,j} + d\alpha_{i,j}) = 0. \end{aligned} \quad (63)$$

Without the stream function representation, the unknowns are each component of the eddy currents at all grid points, hence the number of unknowns is $2m \times n$. However, the number of equations is $m \times n + 1$, implying that the equations are insufficient to solve the problem. By combining the Eq. (63) with the eddy current equation, the solution should be derived if the number of equations equals the number of unknowns. The Eq. (63) can be formulated at each grid intersection point, but they are not completely independent. An equation at a point can be obtained by adding or subtracting the equations at all other points. Therefore, the number of equations from Kirchhoff's first law is only $m \times n - 1$. These $m \times n - 1$ equations can be expressed as the product of the current array

$$[J] = \begin{bmatrix} J^\alpha \\ J^\beta \end{bmatrix}, \quad (64)$$

and the coefficient matrix $[K]$ as

$$[K][J] = 0. \quad (65)$$

The eddy current equation in matrix form (51) can also be expressed without the stream function as

$$\frac{\partial}{\partial t}[L] = [R] - \left[\frac{\partial B_{\text{ex}}^s}{\partial t} \right], \quad (66)$$

$$[L] = \begin{bmatrix} M_{LJ^\alpha} & M_{LJ^\beta} \end{bmatrix} [J] \equiv [M_{LJ}] [J], \quad (66)$$

$$[R] = \begin{bmatrix} M_{RJ^\alpha} & M_{RJ^\beta} \end{bmatrix} [J] \equiv [M_{RJ}] [J], \quad (67)$$

where $[M_{LJ^\alpha}]$, $[M_{LJ^\beta}]$, $[M_{RJ^\alpha}]$, and $[M_{RJ^\beta}]$ are the coefficient matrices in $m \times n - 1$ rows and $m \times n$ columns respectively, and then $[M_{LJ}]$ and $[M_{RJ}]$ have $m \times n - 1$ rows and $2 \times m \times n$ columns. When Eqs. (51) and (65) are combined, the number of equations becomes $(m \times n + 1) + (m \times n - 1) = 2 \times m \times n$, which corresponds to the number of unknowns. Kirchhoff's first law must be applied to the eddy currents at the following time step when doing the computations as

$$\begin{bmatrix} M_{LJ} \frac{\partial J}{\partial t} \\ KJ_{t+\Delta t} \end{bmatrix} = \begin{bmatrix} M_{RJ}J_t - \frac{\partial B_{\text{ex}}^s}{\partial t} \\ 0 \end{bmatrix}. \quad (68)$$

The time derivative of this equation can be discretized in the same way as in Sec. 2.3.6, and the time evolution of the eddy currents can be calculated by performing the time integration with an arbitrary method. As an example, when we adopt the Euler method:

$$[J]_{t+\Delta t} = \begin{bmatrix} M_{LJ} \\ K \end{bmatrix}^{-1} \begin{bmatrix} (M_{LJ} + \Delta t M_{RJ})J_t - \Delta t \frac{\partial B_{\text{ex}}^s}{\partial t} \\ 0 \end{bmatrix}. \quad (69)$$

Note that the computational load for matrix calculation increases when the stream function is not used because each coefficient matrix is of order $2 \times m \times n$, whereas it is of order $m \times n + 1$ when the stream function is used. On the other hand, the number of matrix calculations can be reduced because the calculation to convert the stream function to eddy current is no longer required.

3. Non-Axisymmetric Eddy Current Calculation Code Keddy3D

Based on the computational method described in Sec. 2, we have developed the non-axisymmetric eddy current calculation code Keddy3D. In this section, we describe our simulation setup and calculation results performed to validate the Keddy3D.

3.1 Calculation of axisymmetric eddy current

In eddy current calculation on axisymmetric tokamaks, an approximation method in which the conductor is split into several toroidal conductor loops (filament approximation) [8] is widely employed. We will compare the simulation results of the Keddy3D with those of the filament approximation and establish the validity of axisymmetric eddy current calculations.

3.1.1 Setup

Figure 4 shows a schematic of the vacuum vessel and the center solenoid coils (CS coils) employed in the simulation.

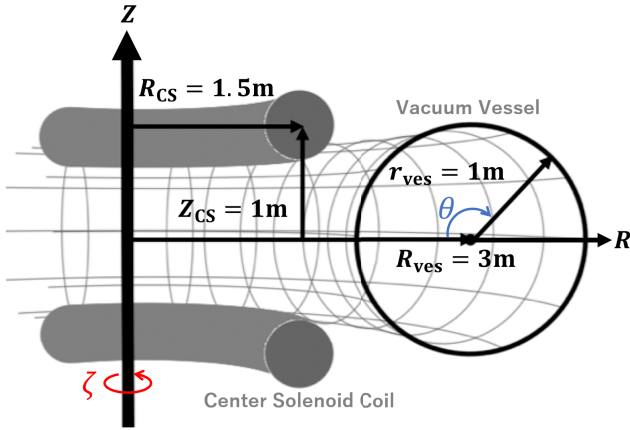


Fig. 4 Simulation setup for axisymmetric eddy current calculation.

The toroidal angle ζ is taken in the direction where the cylindrical coordinate system (R, ζ, Z) is right-handed, and the poloidal angle θ is taken in the direction where the curvilinear coordinate system (s, θ, ζ) is right-handed with the coordinate in the minor radial direction s . Consider a toroidal axisymmetric circular vessel with center point at $(R, Z) = (3 \text{ m}, 0 \text{ m})$, small radius 1 m , wall thickness 0.02 m , and conductivity $0.72 \mu\Omega \cdot \text{m}$. Axisymmetric conductors imitating the CS coils are placed at $(R, Z) = (1.5 \text{ m}, \pm 1 \text{ m})$. The temporal evolution of the induced eddy currents in the vacuum vessel is calculated until it reaches a nearly steady-state. The electromotive force is supplied by flowing currents through each CS coil at a constant time-varying rate of 0.1 MA/s . It is assumed that no eddy currents exist in the initial state. The simulations are carried out with a circuit equation code based on the filament approximation and the Keddy3D, and the results are compared. In the filament approximation code, the vacuum vessel is split into 100 poloidal sections, each of which is considered as an individual axisymmetric conductor. The cross-sectional area of each axisymmetric conductor is adjusted to match the original vacuum vessel's cross-sectional area divided by the number of poloidal sections. In the Keddy3D calculation, the number of grid points in (θ, ζ) direction is set to $(m, n) = (100, 180)$.

3.1.2 Result

The temporal evolution of the total toroidal components of induced eddy currents in the vacuum vessel is shown in Fig. 5.

The total eddy current in Fig. 5 is determined by a simple summation of all currents flowing through the filaments in the filament approximation code. In contrast, an integration of surface current density in poloidal circumference is needed to obtain it in the Keddy3D. According to Fig. 5, it can be seen that the calculated result of the Keddy3D is in good agreement with the result of the filament approxima-

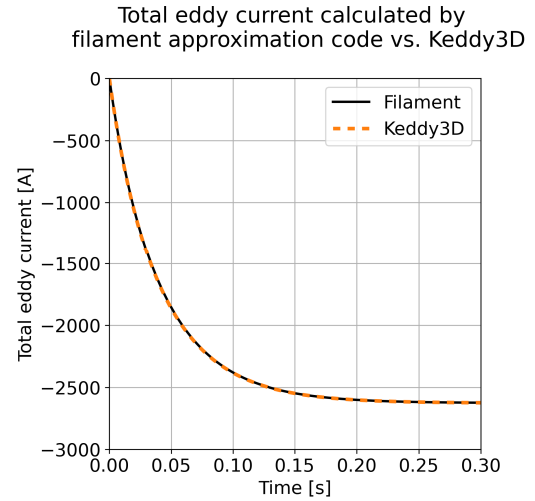


Fig. 5 Time evolution of the total of toroidal eddy currents induced in the vacuum vessel (comparison of filament approximation code vs. Keddy3D).

tion code.

Next, we compare the surface current density distribution of eddy currents at each time. We compare it at three stages of temporal evolution: 0.02 s , 0.10 s , and 0.30 s . The poloidal distribution of eddy current density at each time point is shown in Figs. 6 - 8.

The surface current densities in Figs. 6 - 8 are determined by dividing eddy current values in each filament by the length of the arc to the next filament in the filament approximation code, whereas it is computed as the gradient of stream function in the Keddy3D. The eddy current density distribution has a minor inaccuracy in the early stage of temporal evolution, as seen in Fig. 6. The error is most obvious at $\theta = \pi$ (outboard side of the torus), which can be interpreted as the position away from the evaluation point of the circular voltage equation as the boundary condition. In this simulation, we evaluate the toroidal circular voltage at $\theta = 0$ (inboard side of the torus), and because the circular voltage equation is essentially similar to the circuit equation calculated in the filament approximation, the inaccuracy in the calculation results stays modest at $\theta = 0$. On the other hand, at points other than $\theta = 0$, the Keddy3D evaluates the eddy currents indirectly through the difference of the stream function, whereas the filament approximation obtains the eddy currents from the circuit equation. This discrepancy might be the source of the inaccuracy shown in Fig. 6. The error in the eddy current at $\theta = \pi$ point at 0.02 s was -6.37% when the filament approximation code result was used as the real value. Although this seems to be a significant error, $\theta = \pi$ is the region with the lowest eddy current density, therefore the relative error is easily assessed to be large. As shown in Fig. 6, the overall error is rather minor, and the Keddy3D calculation results are typically consistent with the circuit equation solution (the results of the filament approximation code). Furthermore, Figs. 6 - 8

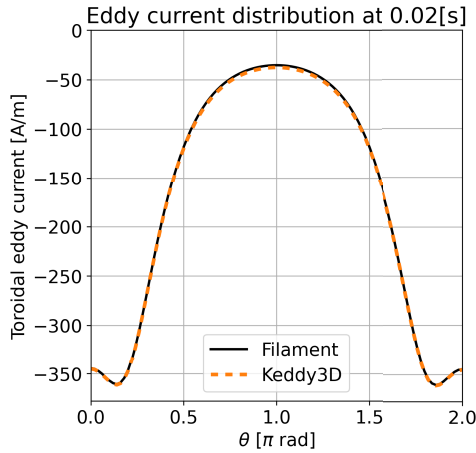


Fig. 6 Poloidal distribution of eddy current density at 0.02 s after simulation start (comparison of filament approximation code vs. Keddy3D).

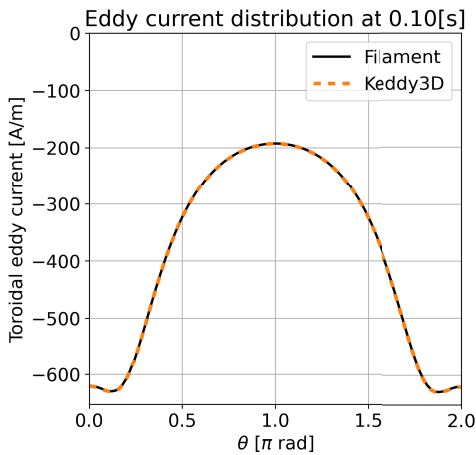


Fig. 7 Poloidal distribution of eddy current density at 0.10 s after simulation start (comparison of filament approximation code vs. Keddy3D).

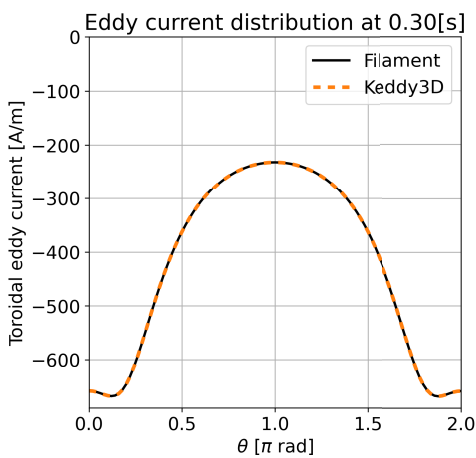


Fig. 8 Poloidal distribution of eddy current density at 0.30 s after simulation start (comparison of filament approximation code vs. Keddy3D).

illustrate that the inaccuracy decreases as the temporal evolution advances. This result suggests that the inaccuracy is mostly attributable to the component of the equation relating to temporal variation, namely $[X]$ in the Eq. (54). This is the term for the magnetic field generated by the eddy currents and is calculated by Biot-Savart’s law. The magnetic field generated by current elements discretized in the toroidal direction in the Keddy3D may differ slightly from the magnetic field generated by continuous currents in the filament approximation code. This discrepancy is assumed to be the source of temporal variation inaccuracies. Actually, the inaccuracy decreases as the number of toroidal grid points n increases, validating the aforementioned assumption.

As a conclusion of this numerical experiment, it was found that the Keddy3D can calculate axisymmetric eddy currents with good overall accuracy, although it is prone to errors in the temporal evolution away from the evaluation point of the boundary condition.

3.2 Calculation of non-axisymmetric eddy current in vessel with bellows

To confirm the validity of the non-axisymmetric eddy current calculations of the Keddy3D, we simulated the case of bellows in a vacuum vessel. In a previous study [9], experimental and simulational results for eddy currents in a tokamak vessel with bellows were compared. Therefore, we can verify the physical consistency of the Keddy3D by comparing the results of the Keddy3D calculations with those of the previous study.

3.2.1 Setup

Figure 9 shows a schematic view of the vacuum vessel and the CS coils employed in the simulation. The CS coils are arranged like the walls of a concentric cylinder, sandwiching the vacuum vessel from the inside and outside.

The wall thickness is set to 8.2 mm in accordance with

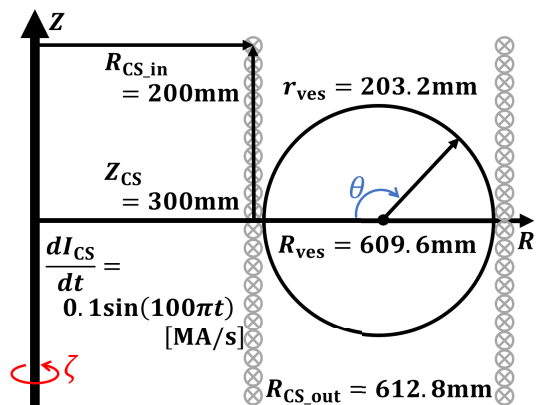


Fig. 9 Simulation setup for non-axisymmetric eddy current calculation.

the previous study [9]. The vacuum vessel has bellows at four separate locations around its circumference, and the vessel is simply modeled by varying the electrical resistivity in the poloidal and toroidal directions at the bellows sites separately. Other experimental settings were not provided in the previous study, thus appropriate values are set by guesswork. The number of grid points in the Keddy3D is set to $(m, n) = (50, 360)$.

We investigate the eddy currents that flow in the vacuum vessel when an alternating current of 50 Hz is supplied to the center solenoid coil.

3.2.2 Result

To begin, we confirm that the eddy current distribution is properly simulated in the presence of bellows. The eddy current distribution in the simulation result of the Keddy3D is shown on the surface of the vacuum vessel by vectors in Fig. 10.

Since the calculation results showed toroidal periodicity, the results are only presented for one cycle, but the entire vessel is calculated. The following three features of the eddy current distribution in the presence of bellows are identified.

1. Because the bellows section has a high electrical resistance in the toroidal direction, currents in the section are small.
2. Large poloidal currents flow along the border between the bellows section and the wall section.
3. Eddy currents circulate through the wall section, forming a saddle-shaped structure.

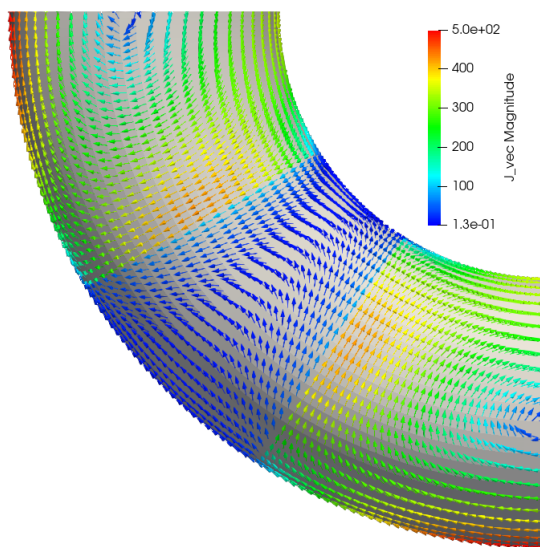


Fig. 10 Result of non-axisymmetric eddy current calculation by the Keddy3D. The direction of a vector corresponds to the direction of the eddy current at its position and the color corresponds to the magnitude of the current.

Looking at Fig. 10, it can be roughly confirmed that the currents are smaller in the bellows section and larger near the boundary and that the currents circulate in the wall section, forming a circulating current flow.

The distribution of eddy currents in each direction is then seen in detail. The current density of the toroidal eddy currents flowing through the vacuum vessel is shown in Fig. 11.

According to Fig. 11, toroidal currents flowing in the bellows section have a consistent direction independent of the poloidal position, but toroidal currents flowing in the wall section have variable directions depending on the poloidal position because they circulate. Comparison with the previous study [9] shows that the magnitude and distribution of the eddy currents are consistent with the experimental result.

Next, the current density of poloidal eddy currents flowing through the vacuum vessel is shown in Fig. 12, taking the distribution in the toroidal direction.

From Fig. 12, we can again confirm the characteristic that the poloidal currents increase near the border between the bellows part and the wall part, which was also observed in Fig. 10. When this result is compared with the previous

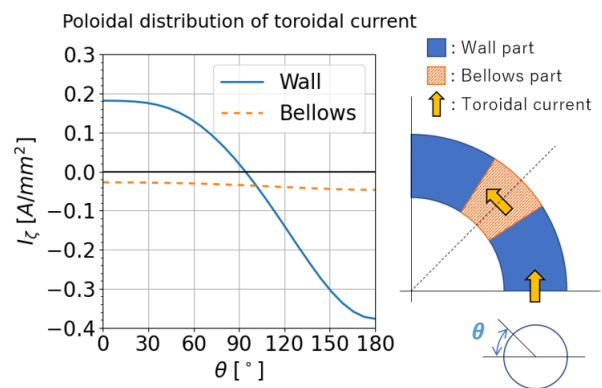


Fig. 11 Poloidal distribution of toroidal eddy current density.

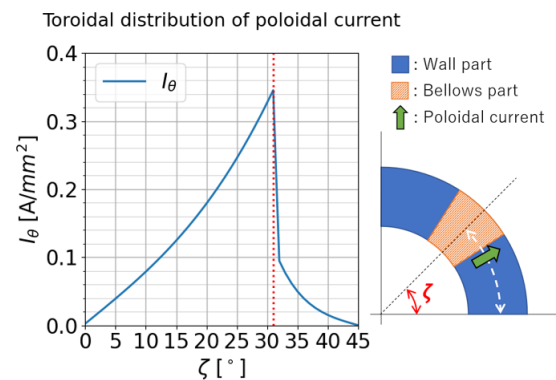


Fig. 12 Toroidal distribution of poloidal eddy current density. The dotted line indicates the boundary between bellows and wall sections.

study [9], the toroidal variation of poloidal current at the boundary between bellows part and wall part ($\zeta = 31^\circ$) is more drastic. The modeling of bellows should be the primary cause of this discrepancy. Because the detailed modeling is not provided in the previous study, we referred to another paper [10] to model the electrical resistivity distribution of bellows. The resistivity in our model discontinuously changes at the boundary in both the poloidal and toroidal directions. The eddy current there varies radically for this reason. The magnitude and distribution of the current are mostly consistent with the experimental result, notwithstanding the gradient's differences.

As a conclusion of this numerical simulation, it can be said that the results of the non-axisymmetric eddy current calculation by the Keddy3D are physically valid since the results generally reproduced the experimental results presented in the previous study.

4. Discussion

The calculation method presented in this study is not suitable for imitating complicated in-vessel components as divertors and blankets precisely because it adopts fixed intervals for the poloidal and toroidal grid, which tend to lack flexibility in spatial expression. However, this study is motivated not to reproduce detailed eddy current structures, but to analyze the dynamics of plasma interacting with the eddy currents. In terms of saving computational resources used by eddy current calculations, we would rather evaluate the effects of the characteristic structures approximately by modeling them as mathematical expressions than imitate them precisely consuming more computing resources by adopting advanced computational methods.

5. Summary

We have developed a new simulation code for simulating the time evolution of non-axisymmetric eddy currents induced on the vacuum vessel. The Keddy3D code solves the eddy current equation obtained by using the thin-wall approximation. In the code, the eddy current is represented in terms of the stream function and is discretized on (m, n) grid points in (θ, ζ) direction, and then the eddy current equation becomes a system of $m \times n - 1$ independent algebraic equations for the stream function at $m \times n + 1$ grid

points. By adding equations for the circulating voltage in each direction, the system of equations becomes solvable.

Two numerical tests are carried out to verify the validity of the Keddy3D code. In the first test, we made the axisymmetric eddy current calculations and compare the obtained results with those from an axisymmetric eddy current calculation code based on the filament approximation. We found that they are in good agreement. In the second test, we simulated eddy currents with non-axisymmetry due to the bellows of a vacuum vessel. We confirmed that the simulation results were consistent with experimental results presented in Ref. [9]. From the results of these numerical experiments, we conclude that the Keddy3D code provides physically reliable results.

The Keddy3D code developed in this study has an advantage in the long-term evolution of non-axisymmetric eddy current on the vacuum vessel because of its low computational cost, and thus the Keddy3D code is useful for the analysis of disruptions and resistive wall modes (RWMs). We have also developed an integrated disruption simulation code that incorporates the Keddy3D code. Our integrated code is capable of performing non-axisymmetric disruption simulations and will be reported in our next paper.

Acknowledgments

This work was supported by QST Research Collaboration for Fusion DEMO and also by the establishment of university fellowships towards the creation of science technology innovation by JST, Grant Number JPMJFS2123.

- [1] Y. Neyatani *et al.*, Fusion Technol. **28**, 1634 (1995).
- [2] R.R. Khayrutdinov *et al.*, J. Comput. Phys. **109**, 193 (1993).
- [3] A. Kameari, J. Comput. Phys. **42**, 124 (1981).
- [4] S. Nishio *et al.*, IEEE Trans. Magn. **26**, 865 (1990).
- [5] M.S. Chu *et al.*, Plasma Phys. Control. Fusion **52**, 123001 (2010).
- [6] J.D. Hanson, Plasma Phys. Control. Fusion **57**, 115006 (2015).
- [7] S. Yamamoto *et al.*, Fusion Eng. Des. **168**, 112361 (2021).
- [8] J.D. Jackson, *Classical Electrodynamics, 2nd Edition*, (Wiley, New York, 1975), 177.
- [9] T. Takahashi *et al.*, Hitachi Hyoron **37**, 53 (1980).
- [10] Y. Nakamura *et al.*, JAERI **1317**, 1–310 (1989).